5
Wafer-Scale Synthesis of a Uniform Film of Few-Layer MoS_2 on GaN for 2D Heterojunction Ultraviolet Photodetector

5.1 INTRODUCTION

The family of 2D-layered materials has recently got huge attention in novel optoelectronics and photovoltaic devices due to their distinct electronic and optical properties (Koppens et al., 2014; Mak and Shan, 2016; Namgung et al., 2016). Graphene proved to be an appealing material for various photodetecting applications because of its ultra-broadband light absorption and fast photoresponse(Liu et al., 2014; Mak et al., 2012). Even though the essential prevalence of graphene cannot be denied, but its poor absorption rate of incident visible irradiation and short photocarrier lifetime make it unsuitable for high-performance photodetectors(Bonaccorso et al., 2010; Li et al., 2014). On the other hand, TMDs are promising photodetecting materials due to their high absorption rate at short wavelengths.

Among various TMDs, MoS_2 is one of the most widely used materials for photodetecting applications. The availability of unsaturated d-orbitals due to molybdenum makes MoS_2 an appealing candidate for several interesting applications. Further, the properties of MoS_2 can easily be tuned by filling of these unsaturated d-orbitals using different methodologies(Canton-Vitoria et al., 2017; Sweet et al., 2017). New functionalities have been observed by using MoS_2 into field-effect transistors, light-sensing, and light-harvesting devices (Lopez-Sanchez et al., 2014; Nourbakhsh et al., 2016). To explore new dimensions, worldwide efforts have been applied to integrate MoS_2 with other 2D and 3D semiconductors forming vdW heterostructures, for instance, MoS_2/Si, MoS_2/WS_2, and MoS_2/SnO(Gong et al., 2014; Li et al., 2014; Wang et al., 2016). The fascinating properties of these heterojunctions, such as dangling-bond-free surface and tunable charge depletion layer, ignited a renewed interest of researches to explore the new exciting physics at the 2D/3D interfaces(Jariwala et al., 2017; Li et al., 2014). Such heterojunctions have demonstrated a significant improvement in the performance of high-speed electronics and light-harvesting devices(Li et al., 2017). However, the precise controlling of doping and producing large area heterostructures with a neat and sharp interface still remains a challenge. Moreover, the few-layer MoS_2 (FL-MoS_2) seems to be more attractive than monolayer MoS_2 particularly for optoelectronic applications due to their wider spectral response(Tsai et al., 2013; Wang et al., 2015). In addition, FL-MoS_2 possesses higher carrier mobility, a greater density of states, and a higher absorption rate of incident photons than single-layer MoS_2(Choi et al., 2012; Liu et al., 2013).

In this chapter, we have demonstrated a 2D/3D based heterostructure and its applications in highly sensitive and very fast ultraviolet (UV) photodetector with excellent performance. The MoS_2/c-GaN based heterojunction was actualized through a two-step process, deposition of a highly controllable and large scalable Mo film by DC-sputtering on top of GaN substrate followed by sulfurization. The heterojunction shows a rectifying behavior, and the movement of carriers across the interface is explained with the energy band diagram. To explore the optoelectronic relevance of FL-MoS_2, the heterojunction was exposed to 365 nm wavelength light irradiation.

5.2 THE GROWTH AND CHARACTERIZATION OF MoS_2/GaN HETEROJUNCTION

5.2.1 Fabrication of MoS_2/GaN heterojunction

The growth of a few atomic layers MoS_2 film on the GaN substrate was carried out by a two-step process. Firstly, a thin film of Mo was deposited on the GaN substrate via magnetron sputtering technique by using a Mo target (99.99 % purity). We have taken a 1×1 cm^2 GaN substrate, which was partially covered by Si_3N_4 (0.5×1 cm^2). Then a window (0.2×0.2 cm^2) was opened on the uncovered GaN substrate using photoresist. A molybdenum film was grown through magnetron sputtering within the predefined window, which was sulfurized to convert it into MoS_2. Therefore, in calculating the responsivity at MoS_2/GaN heterojunction based photodetector, the active area of the device was 4 mm^2. During the growth of Mo film, the DC power, substrate temperature, and Ar gas flow were kept at 40 W, 600 °C, and 40 sccm, respectively. And secondly, the Mo deposited sample was placed in an alumina boat inside the central zone of a 2-inch diameter tube furnace. Another alumina boat containing 1 gm of sulfur was placed at a distance of 12 cm away from the central zone in the horizontal tube furnace. The temperature of the central zone of the furnace was raised from room temperature to 600 °C in 20 min, while the temperature of the other zone containing sulfur was maintained at 220 °C. The furnace was cooled down after 10 min of reaction.

5.2.2 Microscopic and spectroscopic characterizations

The surface morphology of the as-fabricated MoS_2 was examined by field emission scanning electron microscopy (Tecnai G^2 20 (FEI) S-Twin), as shown in Figure 5.1. The FE-SEM images confirm the continuity with the even topography of the as-fabricated MoS_2 film. The white dotted lines in Figure 5.1(a) show that the MoS2 flakes are well connected to one another forming a continuous film. A homogeneous and good quality MoS_2 film was also reaffirmed by the optical images of Figure 5.2(a) and 5.2(b). The optical images showed the large-scale continuous growth of MoS_2 film deposited over GaN substrate.

The structural quality and crystallinity of the MoS_2/GaN heterojunction were characterized by Raman spectroscopy (Renishaw single monochromator with a 514 nm laser excitation) and XRD (Panalytical X Pert Pro) measurements. The XRD peak positions of the as-fabricated FL-MoS2 film at 14.3°, 25.4°, 39° and 58.4° are related to the (002), (004), (103) and (110) faces, respectively, whereas the peak at 34.5° was assigned to the (002) plane of the GaN film (JCPDS card no. 37-1492), as shown in Figure 5.3(a). A relatively strong peak at the (002) peak of the as-fabricated MoS2 confirms the growth of MoS2 along the c-axis with high crystallinity. With the increasing thickness of the MoS2 film, the in-plane vibrational mode in Raman spectra shows a red-shift, whereas the out-of-plane vibrational mode shows a blue-shift in the spectrum. As shown in Figure 5.3(b), the difference of ~24 cm^{-1} between the two vibrational modes confirms the FL-MoS_2.

The XPS and UPS measurements were carried out by Scienta Omicron multiprobe spectroscopy system using monochromatic Al-Kα x-ray radiative source (1486.7 eV) and He I ($h\nu$=21.22 eV) photon source, respectively. XPS analysis was performed to determine the crystal phase, chemical composition and binding energy of the sputtered MoS_2 film. Figure 5.4(a and b) display the XPS spectrum exhibiting core energy levels of Mo and S for the MoS_2 film. A doublet at 229.3 and 232.5 eV related to the 2H phase of MoS_2 is attributed to Mo $3d_{5/2}$ and Mo $3d_{3/2}$ orbitals, respectively. Similarly, an S $2p_{3/2}$ and S $2p_{1/2}$ doublet was observed at 162.2 and 163.3 eV, respectively, which is consistent with 2H-type MoS_2(Qiao et al., 2017). Our results indicate that the as-grown MoS_2 is mainly composed of the 2H phase MoS_2 without the presence of other any other phase. The 2H phase growth occurs due to higher temperature growth, which is highly conducive to the formation of 2H phase MoS_2.

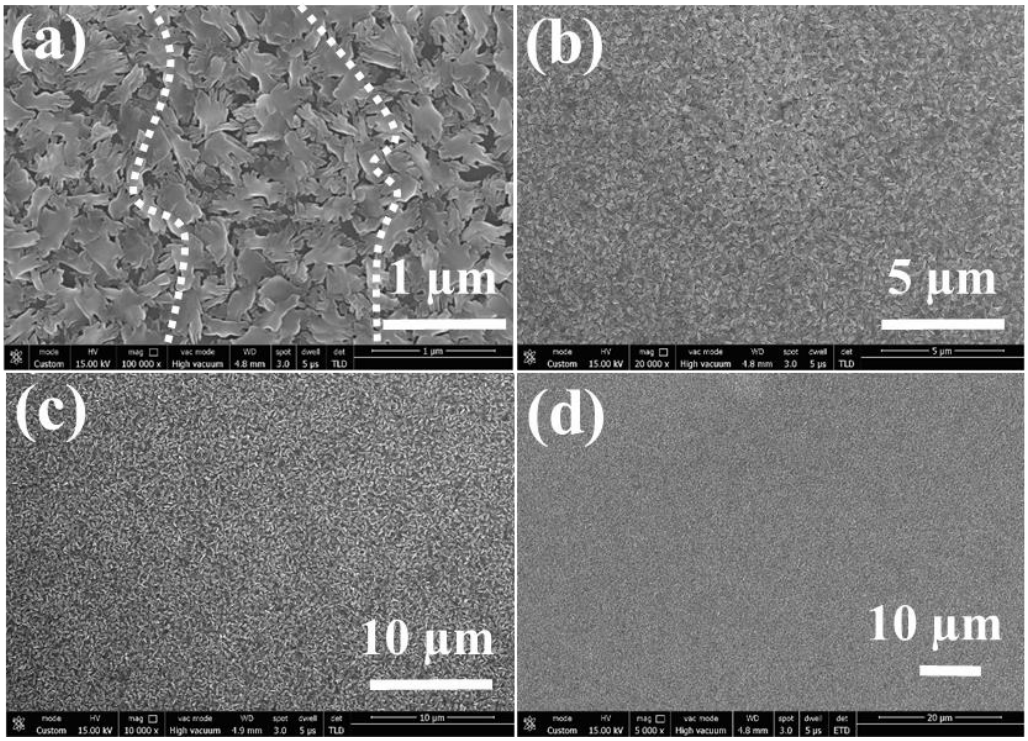

Figure 5.1: (a), (b) SEM micrographs of the MoS_2 film grown on a GaN substrate indicating interconnected MoS_2 flakes.

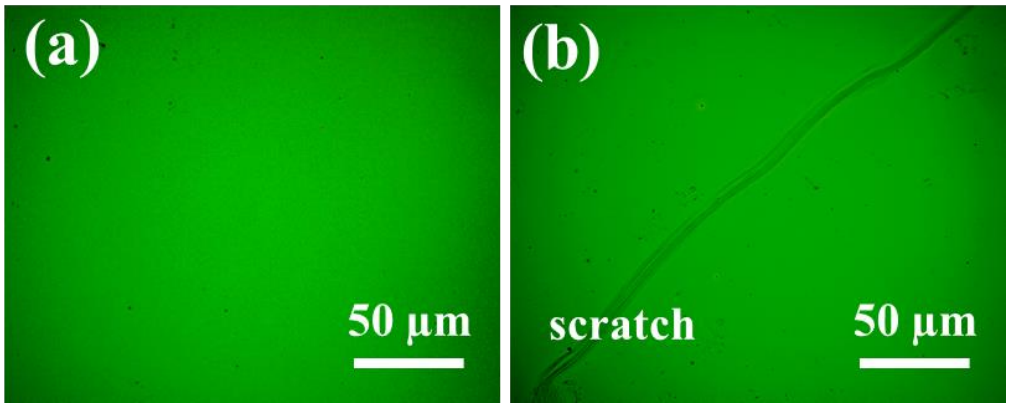

Figure 5.2: (a,b) Optical images of the MoS_2 thin film grown homogenously on GaN substrate, the scratch in penal (b) was intentionally introduced to show the color contrast.

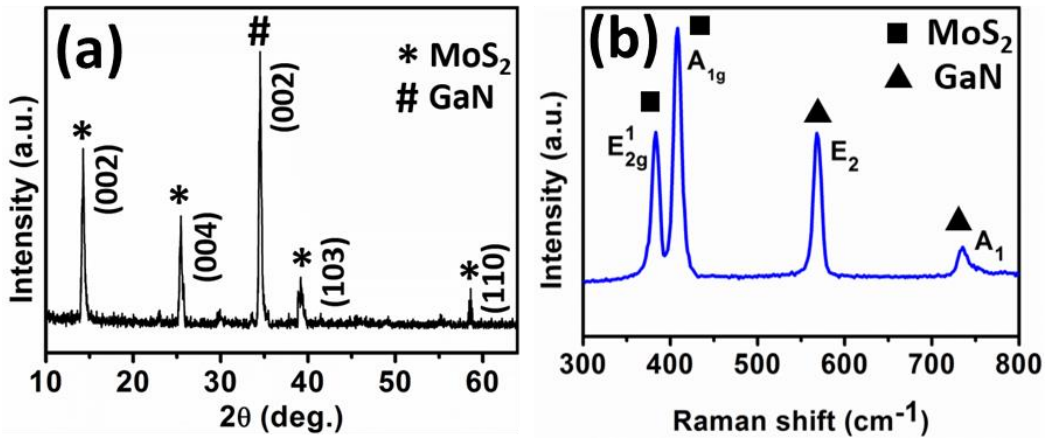

Figure 5.3: (a) The XRD patterns and (b) Raman spectra of the MoS_2/GaN heterojunction.

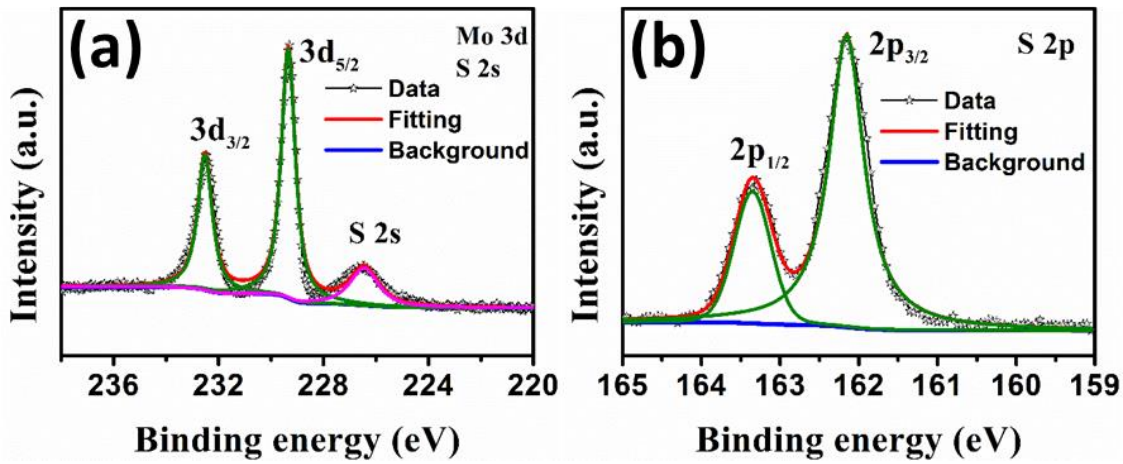

Figure 5.4: An x-ray photoelectron spectroscopy (XPS) analysis of (a) the Mo 3d and (b) the S 2p core regions of MoS_2.

5.2.3 Electrical characterization

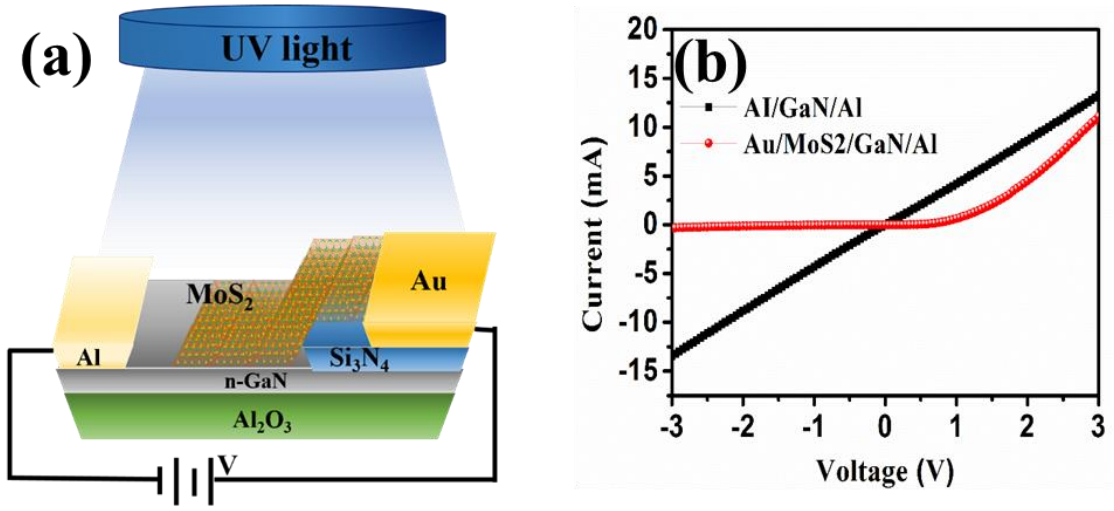

Figure 5.5: (a) Schematic diagram of the MoS_2/GaN heterojunction photodetector device. (b) Current-voltage characteristics of the device without illumination.

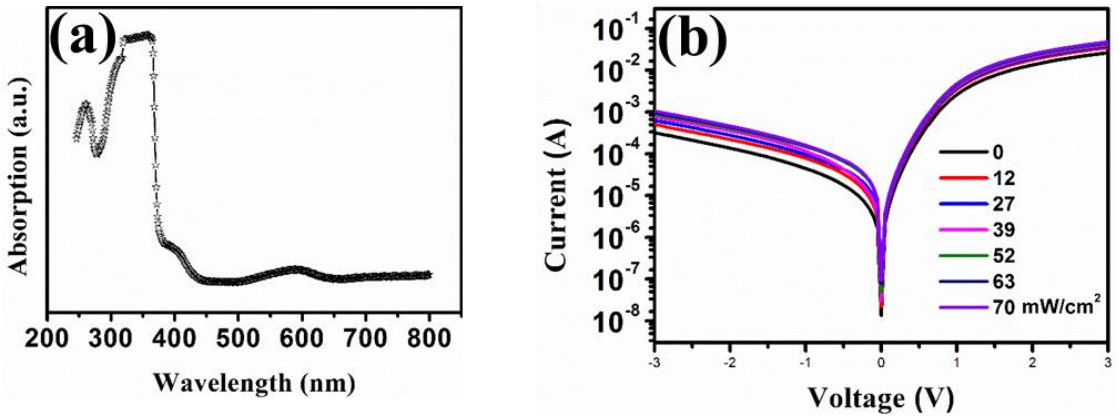

Figure 5.6: (a) UV-Vis absorption spectra of MoS_2/GaN heterojunction. (b) Current-voltage characteristics of the device in dark and under various light intensities.

The schematic diagram of MoS_2/GaN heterojunction based UV photodetector is shown in Figure 5.5(a). The device was annealed at 300 °C for 1 h in Ar ambiance for getting the stable contacts and to minimize the unintentional barrier at the interfaces(Leong et al., 2014). The

current-voltage measurement of the device with an effective area of 4 mm^2 is shown in Figure 5.5(b). The linear behavior of Al/GaN/Al plot in Figure 5.5(b) confirms the ohmic nature of Al on GaN substrate. While Au/MoS_2/GaN/Al exhibit a rectifying behavior due to the presence of MoS_2/GaN heterojunction. Figure 5.6(a) shows the UV-vis spectra of the MoS_2/GaN heterojunction depicting that the maximum excitonic absorption peak lies in the UV region (~360 nm)(Zhuo et al., 2018). The optoelectronic behavior of the device under 365 nm light irradiation of varying intensities (0 to 70 mW/cm^2) is shown in Figure 5.6(b). On careful inspection of Figure 5.6(b), it was observed that under light irradiation, the change in current in the reverse biased mode of operation is more prominent as compared to the forward-biased mode of operation.

5.3 PHOTODETECTING PERFORMANCE OF MoS_2/GaN HETEROJUNCTION

To investigate the performance of our MoS_2/GaN photodetector, the intensity-dependant photoresponse of the device was shown only under reverse bias mode of operation (Figure 5.7(a)). As the power intensity increases from 0 to 70 mW/cm^2, the photocurrent also increases sharply. The spot diameter of our UV light source is approximately 1 cm while keeping the light source at a distance of 1 cm. A steep change in current was observed under the smaller value of illumination intensity. Whereas under high power intensity, a moderate change in current was observed as all the photoinduced charge carriers cannot be separated by the electric field. Moreover, the time-resolved photoresponse was obtained by periodically switching 365 nm optical signal on and off at a fixed voltage bias of –3V. The current increases to its higher values when the UV illumination was turned on for 10 s and regained its original value after turning off the illumination for next 15 s. Time-resolved photoresponse of the MoS_2/GaN heterojunction under different biasing of 0.5, 1.0, 1.5, and 2 V is shown in Figure 5.7(b-f). A very fast response is depicted by the steep rising and falling edges of the photoinduced current. A rise and decay time of 5.4 and 5.6 ms were obtained, as shown in Figure 5.7(d). This fast response is ascribed to the effective separation of generated photoinduced charge carriers at the MoS_2/GaN interface. Our results reflect that the photodetector possesses good stability and high reproducibility with a tuneable photo-dark current ratio.

There is various kind of interfacial gating mechanisms occurring in heterostructure based devices, including photoconductive effect, photogating effect, photovoltaic effect, and photothermoelectric effects. In general, photovoltaic and photoconductive effects play a dominant role in the sensing mechanism of photodetectors. These interfacing phenomena modulate the conductance of the channel resulting in a change in device current and hence a strong photogain. The photovoltaic effect occurs without applying any external biasing (at no bias). While in the photoconductive mode device works under reverse biasing condition(Xie et al., 2017). Under light irradiation, the incident photons generate the free charge carriers. The built-in and externally applied electric field facilitates the separation of photoinduced charge carriers and hence a net increase in the device current. In most of the cases, the photovoltaic and photoconductive effects, both the phenomena often occur simultaneously in photodetectors under reverse bias condition, leading to a high value of photoresponse. So, it is very difficult to disentangle their individual contributions(Furchi et al., 2014).

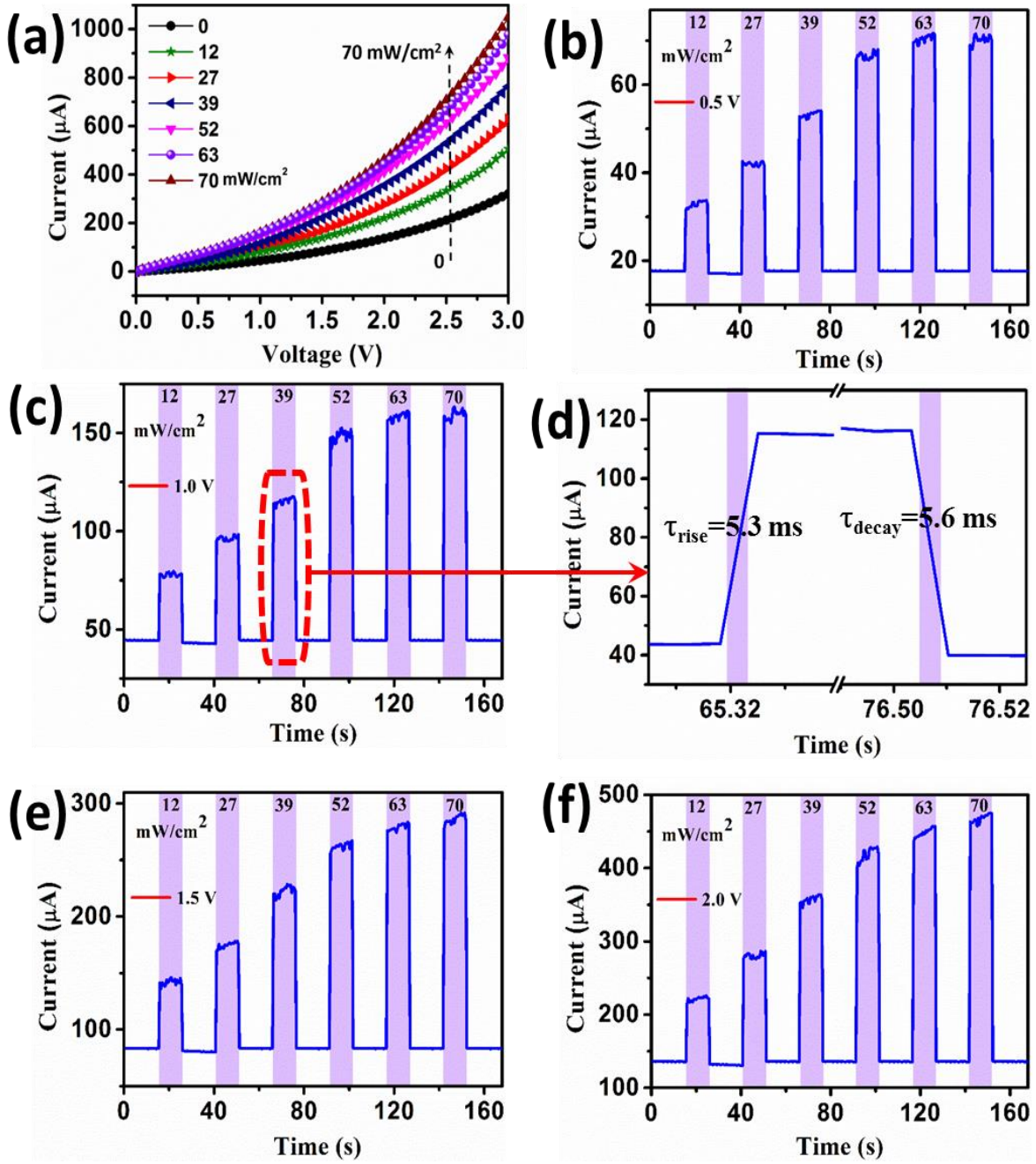

Figure 5.7: (a) The current–voltage characteristics of the MoS_2/GaN heterojunction based photodetector measured in the dark and under light irradiation with different light intensities under reverse bias condition. (b-f) Photo switching characteristic of the device under 365 nm light irradiation with different light intensities at the bias voltage of 0.5, 1, 1.5, and 2V. The light was turned on/off regularly to measure the time-dependent response of the photodetector. (d) Shows the enlarged rising and falling edges with a very fast rise (τ_{rise}) and decay (τ_{decay}) time of 5.3 and 5.6 ms, respectively.

5.4 FIGURES OF MERIT OF MoS_2/GaN PHOTODETECTOR

It was observed that the photocurrent is strongly dependant on the intensity of the incident light irradiation, and it increases with an increase in light intensity (Figure 5.8(a)).

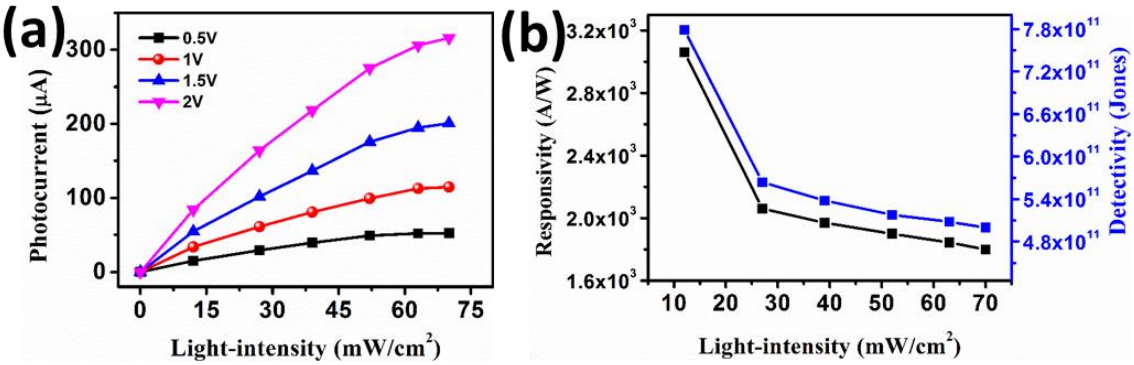

Figure 5.8: (a) The photocurrent as a function of light-intensity under different voltage bias conditions. (b) Responsivity and detectivity measured at the bias of 1 V with different incident light-intensity.

External photoresponsivity, specific detectivity, and response time are widely accepted key parameters for evaluating the performance of a photodetector. The photoresponsivity (R) indicating the ratio of photocurrent to illumination power is given by the following expression(Choi et al., 2014):

$$R = \frac{I_{ph}}{P_{in}} \tag{5.1}$$

where I_{ph} is the photocurrent and P_{in} is the incident optical power on the active area of the device. Using Eq. 5.1, we have achieved a higher photoresponsivity of 3×10^3 A/W at 1V under a light intensity of 12 mW/cm^2, which is significantly higher than earlier reported values of MoS_2 and GaN-based photodetectors (Table 5.1). A high value of photoresponsivity indicates a higher value of photocurrent gain under the relatively smaller value of optical signal. To determine the optical signal detecting ability of our photodetector we calculated the specific detectivity (D^*), under the assumption that the shot noise from dark current is the major contributor to the total noise, which is given by the following equation(Choi et al., 2014):

$$D^* = \frac{S^{1/2}R}{(2qI_d)^{1/2}} \tag{5.2}$$

where S is the active area of the photodetector, q is the electronic charge, and I_d is the dark current. In the calculation of detectivity, the dimensions and noise of the device have to be taken into consideration. There are three factors limiting the detectivity of the photodetectors, they are shot noise, thermal noise, and flicker noise(Gong et al., 2009). In our calculation of specific detectivity, we assumed that the dark current is dominated by the shot noise. Although in addition to shot noise, the other factors such as thermal noise and flicker noise also occurs due to thermal fluctuations. However, the values of these other sources are significantly lower than that of shot noise, particularly at the small value of reverse biasing(Fang et al., 2019). We have applied a low reverse biasing voltage (-3V) and hence neglected the thermal and flicker noise. Moreover, a lower value of series resistance also reduces both the thermal noise flicker noises(Li et al., 2017). Thus, by optimizing the synthesizing and processing technique, these factors could further be reduced. A large number of published articles on photodetectors also calculated the value of detectivity from the root mean square of the shot noise only. The current noise spectra in the earlier reports also confirm that the dark current is dominated by the shot noise(Guo et al., 2012; Ma et al., 2016). Based on Eq. 5.2, specific detectivity of the MoS_2/GaN heterojunction is calculated to be ~ 10^{11} Jones under UV illumination of varying intensity. The estimated value of detectivity is comparable with other MoS_2 based photodetectors (Table 5.1). Figure 5.8(b) shows the responsivity and detectivity of the MoS_2/GaN heterojunction at 1 V under the illumination of different wavelengths. At 1 V, R varies between 3.05×10^3-1.8×10^3 A/W, whereas D^* is of the order of ~10^{11} Jones. The spectral photoresponsivity is more

prominent at a smaller value of light intensity, as shown in Figure 5.8(b). It was observed that both responsivity and detectivity decrease with an increase in light intensity, which is due to existence of trap states at the MoS_2/GaN interface and in the MoS_2 film. The photoinduced charge carriers will get quenched by the trap states under low light intensity, which leads to reduced recombination rate and an improved lifetime of the photo-excited carriers. However, increasing the light intensity results in decaying the number of trap states leading to saturation of the photocurrent(Xu et al., 2014).

5.5 CHARGE TRANSPORT MECHANISM AT MOS_2/GaN HETEROINTERFACE

The charge transport mechanism across the MoS_2/GaN interface can also be understood by energy band diagram at the heterojunction. Once the heterojunction is formed between MoS_2 and GaN, the band alignment at MoS_2/Si heterojunction would be as shown in Fig. 5.9(a), under an equilibrium condition. Whereas under the reverse bias condition, electrons from the MoS_2 side will move towards the GaN, as depicting is Figure 5.9 (b). Therefore, the movement of charge carriers due to the difference in fermi levels results in downward bending of MoS_2 surface and upward bending of GaN surface. Under UV-excitation, e-h pairs are generated due to absorption of incident photons at the heterojunction. The photogenerated charge carriers are separated by the electric field present at the interface contributing to the photocurrent.

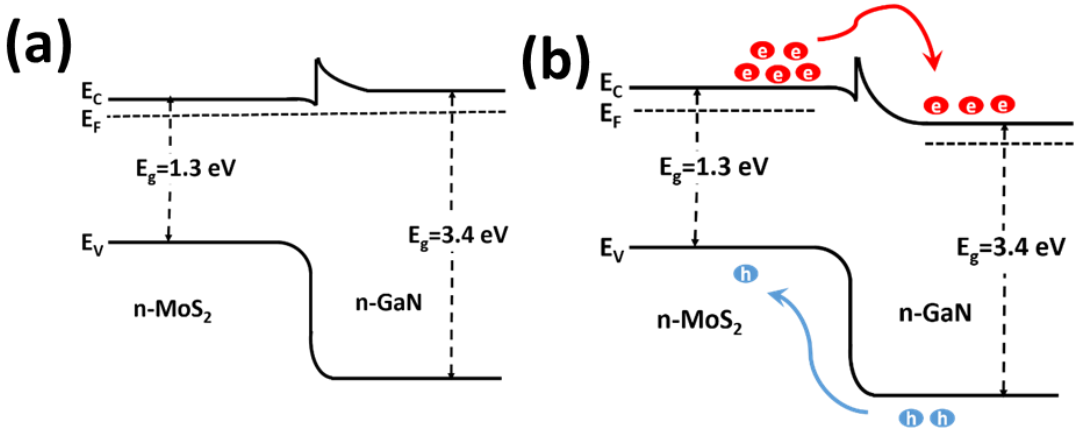

Figure 5.9: (a) Energy band diagram of the MoS_2/GaN heterojunction under equilibrium and (b) under reverse bias condition showing the process of charge transfer at the junction between MoS_2 and GaN by light illumination. The bandgap (E_g) of MoS_2 and n-GaN is 1.3 and 3.4 eV, respectively. E_C, E_F, and E_V denote the bottom of the conduction band, Femi level, and top of valence band, respectively.

5.6 CALCULATION OF BARRIER HEIGHT AT THE MOS_2/GaN HETEROINTERFACE

The barrier height at the rectifying MoS_2/GaN interface could be calculated by Bardeen's model using the I-V characteristic of the heterojunction. In accordance with the proposed model, the barrier height at the interface decays linearly with an increase in the electric field. The reverse-biased barrier height under the light irradiation of different intensities could be described as per the following relation(Ranwa et al., 2014; Zhang and Harrell, 2003):

$$I = I_0 exp\left(\frac{\beta\sqrt{V}}{kT}\right) \tag{5.3}$$

and the reverse saturation current I_0 is given by:

$$I_0 = SA^* exp\left(-\frac{q\Phi r}{kT}\right) \tag{5.4}$$

where β is the interface related parameter, V is the applied reverse voltage, k is the Boltzmann's constant, and T is the operating temperature. S is the active area, A^* is the effective Richardson's constant (26.4 A/cm^2.K^2 for n-GaN substrate), and Φ_r is the reverse barrier height(Kumar et al., 2013). Using Eq. 5.3 and 5.4, we evaluated Φ_r by fitting the experimental

data shown in Figure 5.7(a). The calculated values of Φ_r vary from 0.395 to 0.349 eV as the intensity changes from 0 to 70 mW/cm^2. Figure 5.10 shows that the value of barrier height decreases with an increase in illumination intensity. Our obtained results are consistent with the earlier reported results(Liu et al., 2008; Lu et al., 2015).

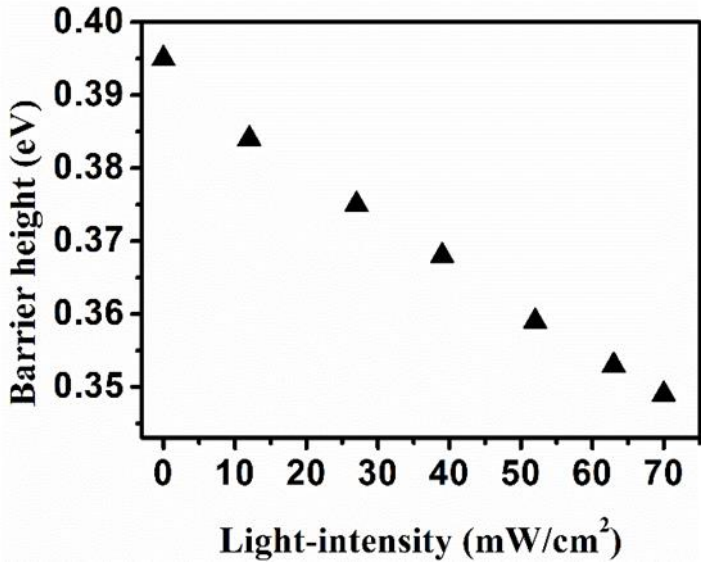

Figure 5.10: Barrier height as a function of light intensity at the MoS_2 and GaN interface.

Table 5.1: Performance comparison of our MoS_2/GaN based photodetector with that of already reported MoS_2 and GaN-based photodetectors

Device	Photoresponsivity (A/W)	Detectivity (Jones)	Response time	Wavelength (nm)	Ref.
MoS_2/GaN heterojunction	≈10^3	≈10^{11}	5 ms	365	This work
MoS_2 p–n junction	5.07	3×10^{10}	150 ms	400	(Choi et al., 2014)
Self-Aligned MoS_2 FET	734.5	–	5 ms	550	(Liu et al., 2016)
MoS_2/GaN heterojunction	–	–	66 ms	365	(Xue et al., 2017)
MoS_2 FET using surface treatment	1.98	6.11×10^{10}	0.3 s	405	(Pak et al., 2015)
Multilayer MoS_2–WS_2 Heterostructure	1.42	–	–	633	(Huo et al., 2014)
APTES/MoS_2 transistors	5.75×10^3	4.47×10^9	–	655	(Kang et al., 2015)

Few-layered MoS_2 MSM photodetectors	0.57	10^{10}	70 µs	532	(Tsai et al., 2013)
GaN-based detector	0.104	–	10 ms	360	(Sun et al., 2015)
GaN Nanowire UV Photodetector	70.4	–	–	360	(Weng et al., 2011)
n-ZnO/p-GaN Heterojunction	4×10^{-7}	1.41×10^{8}	–	374	(Zhu et al., 2008)
$CH_3NH_3PbI_3$/GaN Heterojunction	0.198	7.96×10^{12}	0.34 s	500	(Zhou et al., 2017)

The above results clearly demonstrate the importance of MoS_2/GaN heterojunction for high-performance UV photodetectors. Table 5.1 indicates the significantly higher performance characteristics of our MoS_2/GaN based photodetector as compared to that of earlier reported MoS_2 and GaN-based photodetectors. However, the response speed of the photodetector can further be improved by reducing the active area of the device as the larger device size will lead to a greater value of RC constant, which results in slower photoresponse. The sputtering method employed for making the growth of large -scale FL-MoS_2 is expected to be equally applicable to other 2D materials, thus paving the way for scalable 2D/3D hybrid photodetectors with excellent performance.

5.7 CHAPTER SUMMARY

MoS_2/GaN heterojunction based UV photodetector was actualized by growing large-scale MoS_2 using DC sputtering followed by sulfurization, on top of GaN substrate. The MoS_2/GaN heterojunction exhibits a rectifying behavior with a barrier height of 0.395 eV without illumination. The I-V characteristics measured by varying the light intensity of the incident irradiation from 0 to 70 mW/cm^2 indicate that illumination strongly influences the barrier height at the interface. The FL-MoS_2 is advantageous than its monolayer and multilayer counterpart in terms of its higher light absorption capacity and fast generation and separation of the photo-induced charge carriers. Thus, fabrication of wafer-scale continuous MoS_2 film deposition, with the high performance of MoS_2/GaN photodetector, opens up new avenues for manufacturing multifunctional devices by the integration of 2D materials with bulk 3D semiconductors.

…